

Hyper-Raman scattering from the LO modes of perovskite ferroelectric relaxors

A. Al-Zein^{1,2,*} and B. Hehlen³

¹Department of Physics, Faculty of Arts and Sciences, *University of Balamand, Kelhat, Deir El Balamand, PO box 100 Triploi, Lebanon*

²Electrical and Computer Engineering Department, *American University in Dubai, PO Box 28282, Dubai, UAE*

³Laboratoire Charles Coulomb, UMR 5221, CNRS and *Université Montpellier II, F-34095 Montpellier, France*



(Received 4 April 2024; accepted 28 June 2024; published 22 July 2024)

Hyper-Raman scattering is used to study the temperature dependence of the longitudinal optic (LO) modes of three prototypical ferroelectric relaxors in a broad temperature range from 20 to 800 K. The three LO bands observed in all spectra of the three materials are linked to the three transverse optic (TO) modes in cubic relaxors where LO_{*i*} is linked to TO_{*i*}, with *i* = 1 to 3. The Last, Slater, and Axe eigenvector pictures of the TO modes are consistent with our observations on LO1, LO2, and LO3, respectively. Within this framework, the splitting of LO2 would mostly be linked to a structural disorder on the *B* site while the strength of an anomaly of LO1 near the freezing temperature *T_f* relies on the ability of the material to develop a long-range ordering. Moreover, the more pronounced the splitting, the more important the structural disorder and the lower the value of the dielectric constant.

DOI: [10.1103/PhysRevB.110.024313](https://doi.org/10.1103/PhysRevB.110.024313)

I. INTRODUCTION

For more than 70 years, scientists have been trying to understand and describe the structure and the mechanisms underlying the series of phase transitions in ferroelectric relaxors. [1,2]. The main challenge is that the latter have an ordered crystalline-like average structure but strong local disorder due to off-center ions with respect to the crystalline lattice sites [3–7]. This is due to the fact that most of the widely used relaxors are complex oxide perovskites with two different cations, *B'* and *B''*, occupying the *B* site of the *ABO*₃ lattice. The random substitution of *B'* and *B''* gives rise locally to a strong chemical and mass disorder leading to the intrinsic positional atomic disorder of these materials [3,8].

At very high temperatures, thermal fluctuations are large and all relaxors are in the paraelectric state of cubic average symmetry. Upon cooling, the nucleation of randomly oriented polar nanoregions (PNRs) [9] starts near a singular temperature known as Burns temperature *T_d* [10,11]. This is accompanied with a transformation from a paraelectric phase to ergodic relaxor state [12,13]. However, the absence of charge compensation between the ions of *B'* and *B''* leads to the appearance of very strong local electric fields. It is these random fields together with the strong structural disorder which probably prevent a long-range order. Below *T_d*, the motion of the PNRs slows down until they are completely frozen below a temperature *T_f*, where there is a transition to a nonergodic state [12].

A similar kind of nonergodicity is a characteristic of a dipole glass phase [14,15]. The existence in relaxors of an equilibrium phase transition into a low-temperature glassy phase is one of the most interesting hypotheses which have been discussed intensively. The dielectric constant exhibits a strong diffuse behavior characterized by a temperature- and frequency-dependent maximum [16–18]. This maximum occurs at a temperature *T_m* which does not correspond to a structural phase transition from the paraelectric to ferroelectric state similar to the Curie point *T_C* in normal ferroelectrics [16].

Lead magnesium niobate $\text{PbMg}_{1/3}\text{Nb}_{2/3}\text{O}_3$ (PMN) [19,20] is a typical representative of ferroelectric relaxors. It has an average *Pm* $\bar{3}m$ cubic symmetry down to the lowest temperature. At the nanometric scale, the PMN crystal has a lower symmetry owing to the random distribution of the Mg^{2+} and Nb^{5+} ions occupying the *B* site of the perovskite and due to the short- or medium- range displacement order of PNRs that appear near Burns temperature *T_d* \approx 630 K [21]. The formation of polar nanodomains near *T_d* translates into the deviation of the thermal expansion [22] and the refractive index [21] from their standard linear behavior. The temperature dependence of the acoustic emission from PMN crystals shows two quite sharp peaks near 500 and 630 K correlating with another singular temperature *T** [19,23] and *T_d*, respectively. The dielectric permittivity of PMN crystals shows a typical relaxor behavior with a broad and frequency-dependent peak where the maximum temperature *T_m* is \approx 270 K at 10 kHz [24]. A ferroelectric phase transition in the vicinity of the freezing temperature *T_f* = 220 K [25] can be induced under the application of an electric field that exceeds a threshold value.

At ambient conditions, lead magnesium tantalate $\text{PbMg}_{1/3}\text{Ta}_{2/3}\text{O}_3$ (PMT) [26] possesses an average cubic structure of the *Pm* $\bar{3}m$ space group with a lattice parameter *a* = 4.04 Å [27]. A high-temperature neutron powder diffraction experiment [28] of PMT revealed that there is no

*Contact author: alialzein@gmail.com

structural phase transition in the temperature range from 1.5 to 730 K. In contrast to PMN, PMT remains cubic even if an external electric field is applied [28]. It exhibits the usual relaxor behavior with a $T_m \approx 170$ K at 10 kHz [26,29]. A value of the Burns temperature, $T_d \simeq 570$ K, was estimated from a comparative Brillouin scattering experiment between PMT [29] and PMN [30,31]. However, both the lattice parameter a [28] and the inverse of the dielectric constant ϵ^{-1} [32] of PMT show a deviation from their linear behavior around 420 K, which means that the value of T_d of PMT is still questionable.

Lead zinc niobate $\text{PbZn}_{1/3}\text{Nb}_{2/3}\text{O}_3$ (PZN) [33] is another prototypical relaxor. The temperature dependence of its dielectric constant at different frequencies along the [111] direction shows a typical relaxor behavior with $T_m \approx 410$ K [34]. Contrary to PMN and PMT, a spontaneous phase transition from a cubic to a rhombohedral phase occurs in PZN within the temperature range corresponding to the maximum of $\epsilon(T)$. It was first stated that this transition takes place around 410 K [35,36], but a high-resolution x-ray diffraction study on single crystals shows that this transition is diffuse and spreads over the temperature range between 385 K and 325 K with a full establishment of the rhombohedral phase below 325 K [37]. In addition, high-energy x-ray diffraction measurements [38,39] revealed that the freezing temperature T_f of PZN crystal is ≈ 385 K. The acoustic emission signals from PZN crystal [23] show two sharp peaks near 500 and 740 K corresponding to T^* and T_d , respectively.

In addition to the usual structural techniques, spectroscopic methods sensitive to vibrational modes are widely used to elucidate phase transition mechanisms. Numerous studies have been already performed using inelastic neutron scattering [40,41], Raman scattering (RS) [42–44], and infrared reflectivity (IR) [19,45,46]. Owing to the local disorder, it is difficult to disentangle the numerous vibrational bands observed in the inelastic scattering spectra of relaxors. For example, within the $Pm\bar{3}m$ cubic space group, the irreducible representation of the modes reads $3F_{1u} + F_{2u}$, where the triply degenerated F_{1u} -symmetry vibrations are polar and the triply degenerated F_{2u} -symmetry mode is nonpolar and involves only the oxygen atoms. All of these modes should be inactive in RS. On the contrary, the Raman spectra of PMN exhibits a series of broad bands, some being associated to first-order scattering processes. Some of these unexpected bands are evidence for the lifting of the cubic selection rules due to the local structural disorder which persists at temperatures well above the Burns temperature [42]. It is sometimes interpreted assuming a local tetragonal distortion leading to a splitting of the three triply degenerated F_{1u} modes into $E + A$ components, both in IR absorption [47] and in hyper-Raman scattering (HRS) [48,49].

In this work, HRS is used to study temperature dependence of longitudinal optic (LO) modes in the ferroelectric relaxors PMN, PMT, and PZN. According to basic selection rules, all polar modes are active in HRS, providing a powerful experimental tool to probe spectral lines down to frequencies of a few cm^{-1} . These unique characteristics provide an alternative way to study the behavior of the vibrational spectra of relaxors in the function of temperature, especially for the low-frequency soft modes [48,50–53]. In the following, the

experiments will focus on LO modes as a probe to study the local disorder and the onset of phase transitions.

II. EXPERIMENTAL DETAILS

HRS is a very powerful vibrational tool which nicely complements RS and infrared absorption (IR) [54,55], due to the specificity of its selection rules. This is even more true in partially disordered and amorphous materials, where the structural disorder (partially) lifts the crystalline selection rules, and for the study of low-lying vibrations such as the polar ferroelectric soft modes which are difficult to access using IR [50]. HRS is a three-photon process where two incident photons produce one scattered photon after interaction with an elementary excitation in the material (e.g., vibration or relaxation motions). For HRS, the law of conservation of energy relates the incident frequency ω_i , the scattered frequency ω_s , and the vibrational frequency ω , where $\omega_s = 2\omega_i \pm \omega$.

Unpolarized hyper-Raman spectra were collected using a homemade spectrometer [56–58]. A diode-pumped Q-switched Nd-doped yttrium aluminum garnet laser emitting at the wavelength $\lambda = 1.064 \mu\text{m}$ was used as an exciting source. The repetition rates are between 1 Hz and 50 kHz with pulse widths of ~ 30 ns. The incident peak power is kept slightly below the optical damage threshold of the sample, which for most of our ferroelectric samples was about 2 kW. The incident beam is focused on the sample with a lens L_1 of focal length $f_1 = 47$ mm leading to a waist diameter of $\sim 20 \mu\text{m}$. The scattered light is collected by a photo-objective lens L_2 ($f_2 = 50$ mm) of numerical aperture $N_A = 0.45$ followed by another lens L_3 of focal length $f_3 = 230$ mm. Both near-forward scattering and backscattering geometries were used during this study. The HRS spectra are analyzed with a $f/5.6$ Jobin-Yvon FHR-640 single-grating diffractometer of focal length $f = 640$ mm and detected with a nitrogen-cooled charge-coupled-device camera with 2048×512 pixels. Two different gratings were used: one with 600 grooves/mm, giving a resolution of $\sim 6 \text{ cm}^{-1}$ (FWHM) using an entrance slit of $100 \mu\text{m}$, and one with 1800 grooves/mm for high-resolution experiments, giving a spectral resolution of $\sim 2 \text{ cm}^{-1}$ (FWHM) for a $100 \mu\text{m}$ entrance slit into the spectrometer.

III. RESULTS AND DISCUSSION

LO modes usually dominate the HRS spectra of mixed lead-based perovskites [59]. This is particularly true in PMN [60,61] and PMT [49], in which the LOs almost completely mask the signal arising from the transverse optic (TO) modes, even in backscattering where the former are forbidden by symmetry [49] in perfect crystals. To get information on the intensity of the LOs, it is preferable to perform HRS using a geometry where they are allowed by symmetry, as for example near-forward scattering. It was shown in PMN [61] that the ratio between the LO mode strength observed in HRS and the intensity of the corresponding bands in the $-\text{Im}[1/\epsilon]$ spectrum determined from a far-IR experiment is the same for all three main LO bands [45]. This leads to the conclusion that the HRS intensity of the LOs in relaxors mainly arises from the electro-optic (EO) coupling term of the HRS tensor rather

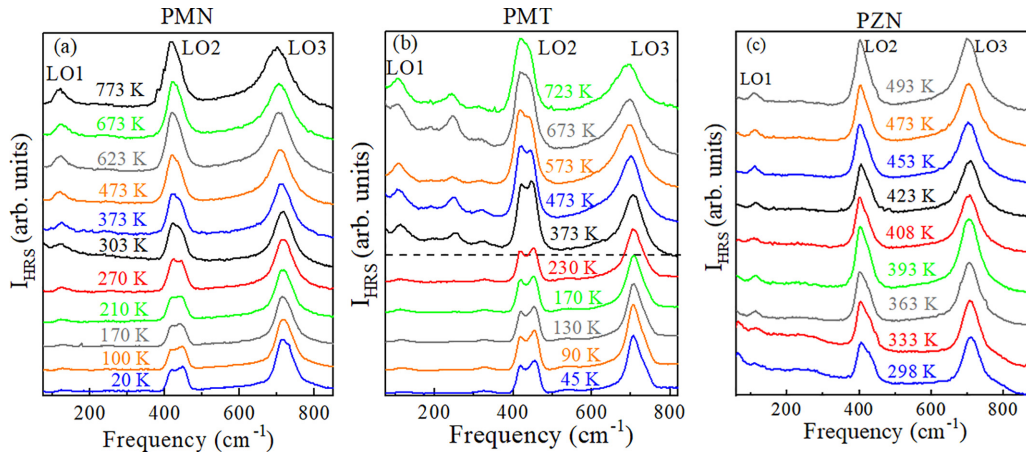


FIG. 1. HRS spectra of PMN (a), PMT (b), and PZN (c) at various temperatures. The PMN spectra, the low-temperature PMT spectra [below the dashed line in (b)], and the PZN spectra are measured in forward-scattering geometry while the high-temperature PMT spectra are collected in backscattering geometry. Note the increasing background in PZN below $T_f \simeq 385$ K due to the superposition of the HRS with a growing Raman signal.

from the deformation-potential contribution. This strong EO coupling in relaxors makes HRS an extremely useful tool for direct experimental observation of the polar LO modes (with their relative strength), otherwise only accessible via fitting or Kramers-Kronig analysis of IR spectra.

Unpolarized HRS spectra of PMN ($q \parallel [001]$), PMT ($q \parallel [001]$), and PZN ($q \parallel [001]$) single crystals at different temperatures obtained with the setup in its low-resolution mode are shown in Fig. 1. The PMN spectra, the PZN spectra, and the low-temperature PMT spectra (below 230 K) were collected in near-forward scattering while the PMT spectra above room temperature were recorded in backscattering geometry. The different experimental geometries used to perform this study prevent a comparison of the intensities of the HRS bands at various temperatures. The ferroelectric transition in PZN induces a growing second harmonic generation (SHG) signal on cooling below T_f . This strong green light induces an RS signal which superposes to the HRS one leading to a structured background below ~ 360 K. This is the reason HRS spectra have not been recorded below room temperature. The three LO bands are clearly seen in all of the spectra: one weak and asymmetric line around 110 cm^{-1} (LO1), a double-peak structure around 400 cm^{-1} (LO2), and a broad Lorentzian-like peak centered around 700 cm^{-1} (LO3). The following subsections describe the temperature behavior of these bands.

A. LO3

The LO3 mode near 700 cm^{-1} can be fitted with a Lorentzian function [inset of Fig. 2(b)], which means that we access the homogeneous width of the vibration. A Gaussian function centered near 600 cm^{-1} is also used to fit the tail in the low-frequency side of LO3. This spectral component likely associates with the high-frequency A_1 mode of the TO3 doublet which is indeed expected in that frequency range [45]. The fit sometimes requires a weak additional contribution centered at $\sim 780 \text{ cm}^{-1}$, suggesting that the band near $\sim 700 \text{ cm}^{-1}$ likely corresponds to the E_1 component of the

LO3 doublet while the weak contribution $\sim 780 \text{ cm}^{-1}$ could eventually correspond to the A_1 component as proposed by IR [45]. The temperature dependence of the frequency ω and the full width at half maximum of LO3 in PMN and PMT are shown in Fig. 2. The dashed lines are guides for the eyes. They mimic standard monotonous behaviors. In PZN, the growth of the Raman signal underneath LO3 below T_f prevents an accurate determination of these quantities.

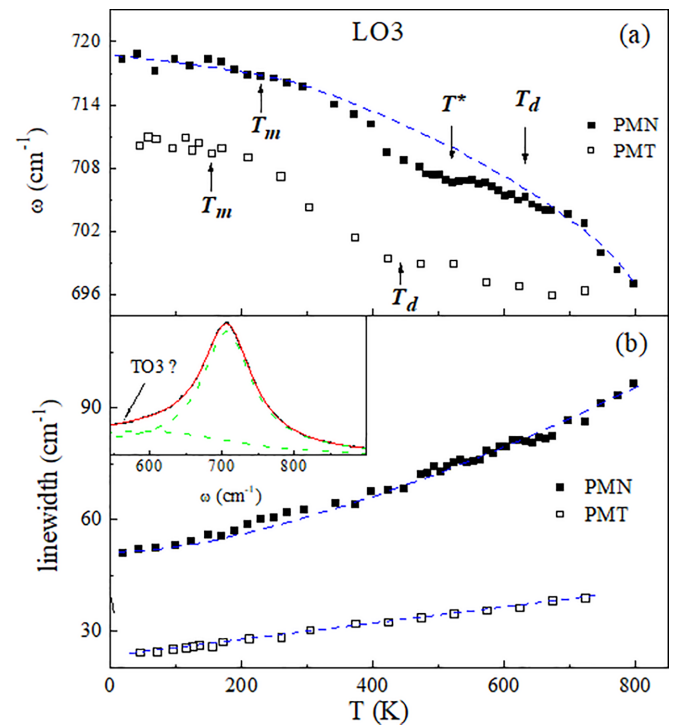


FIG. 2. Temperature dependence of the frequency ω (a) and the linewidth (b) of the LO3 mode for PMN and PMT. The inset shows the fitting of the LO3 mode using a Lorentzian function with a Gaussian function for the tail.

One observes from Fig. 2 that the linewidth of LO3 in PMT is smaller than that in PMN. It is worth noting here that the same trend applies to almost all of the HRS active bands. No observable anomaly can be seen within the full temperature range explored. The temperature dependence of the frequency is more complicated. In PMN, one can eventually see three inflection points [change in the sign of the second derivative of $\omega(T)$]: the first one around T_d , the second one around 500 K (T^* in PMN), and the last one at T_m . This qualitative observation should be taken cautiously, as we do not have any physical model that could explain these effects. Although the dispersion of the points is larger, the same behavior seems to apply in PMT. In any case, these anomalies are very weak (less than 1%), at least compared to those on LO1 and LO2 (see the following).

B. LO2

The low-resolution HRS spectra in Fig. 1 show a clear splitting of the LO2 band in the three materials. This splitting increases as the temperature decreases. To obtain a better observation, high-resolution HRS in PMN was performed. The obtained spectra zoomed on the LO2 region, together with those of PMT, are shown in Fig. 3. For sake of clarity, the spectra have been normalized on top of the low-frequency component.

It is impossible to reproduce the shape of the LO2 doublet with two Lorentzians. The best fit is obtained with two Voigt functions in addition to a sloping background (insets of Fig. 3). This emphasizes an inhomogeneous broadening of the bands due to the structural disorder. The frequencies resulting from the fit are shown in Fig. 4. The low-frequency component [Fig. 4(b)] exhibits a linear temperature dependence in both materials with a larger slope for PMT. As directly evidenced by the raw data (Fig. 3), the frequency of the higher band is much more affected by the temperature. It exhibits in both materials a stiff increase between T_m and T_d [Fig. 4(a)]. This effect is more clear when one plots the frequency shift between the two lines, $\Delta\omega = \omega(A_1) - \omega(E_1)$ [Fig. 4(c)]. This representation has the advantage of avoiding the errors due to slight frequency drifts of the spectrometer. According to the anisotropic dielectric constant model developed by Hlinka *et al.* [45], we associated the low- and high-frequency lines of the LO2 doublet to the E_1 and A_1 modes, respectively. Similarly to the soft mode, the splitting of LO2 persists well above T_d , suggesting that the local structural disorder remains up to very high temperature as already proposed [42].

The data analysis in PZN was done exactly the same way as that for PMN and PMT (same fitting functions and same fitting procedure). Similarly to PMN and PMT, the E_1 component behaves normally [Fig. 5(a)]. However, and contrary to the cubic relaxors, a sharp but reliable anomaly is observed in the temperature dependence of the A_1 component at $T_m \approx 410$ K where the long-range transition from paraelectric to ferroelectric state takes place [34]. This transition-like feature is also clearly visible in a plot of $\Delta\omega = \omega(A_1) - \omega(E_1)$ [Fig. 5(b)]. Unfortunately, owing to possible sample damage, we stopped our experiments at ~ 500 K and thus did not reach $T_d \approx 740$ K. However, a quick observation on the raw data shows that the spectra above T_m are all very similar and that

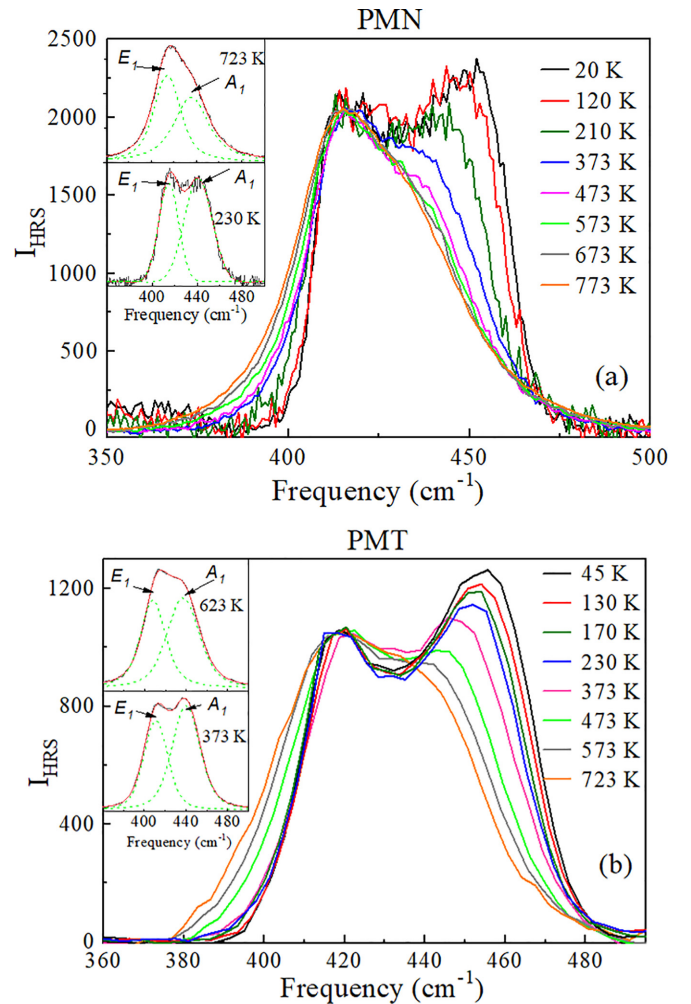


FIG. 3. (a) High-resolution HRS spectra of PMN obtained in forward-scattering geometry at various temperatures. (b) The frequency region of the LO2 mode of the PMT spectra shown in Fig. 1(b). The spectra of PMN and PMT are normalized on top of the E_1 component of LO2. The inset of (a) shows the PMN spectra at 723 K (top) and at 230 K (bottom). The inset of (b) shows the PMT spectra at 623 K (top) and at 373 K (bottom). The red line is the fit resulting from the model described in the text. Dashed lines show the individual contributions corresponding to the E_1 and A_1 components.

the splitting rather develops around T_m or slightly above [inset of Fig. 5(b)]. The situation is clearly different from that of PMN and PMT where the A_1 component starts to increase around T_d and is clearly visible between T_d and T_m . This probably means that the structural disorder is weaker in PZN, thus limiting frustration effect, and consequently favoring a long-range order transition near T_m .

C. LO1

The last longitudinal band to be discussed in Fig. 1 is LO1. This band is clearly asymmetric and cannot be fitted by a single Lorentzian or Gaussian. This asymmetry likely arises from a superposition of the E_1 and A_1 components of the LO1 doublet which cannot be resolved in our experiment. It follows that the frequency of the peak maximum of the band

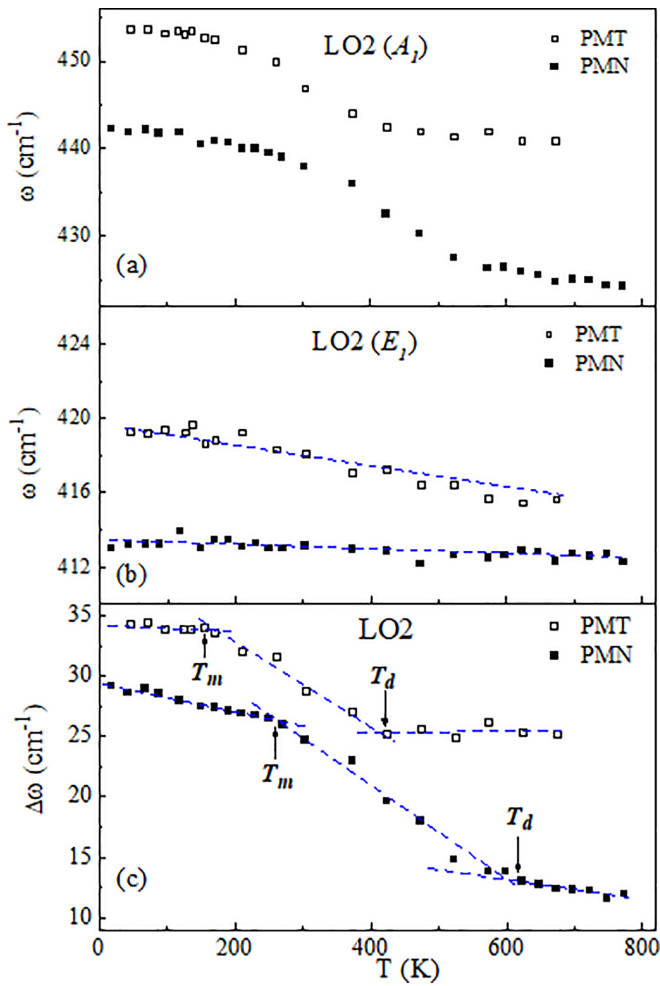


FIG. 4. Temperature dependence of the A_1 (a) and E_1 (b) frequencies together with $\Delta\omega = \omega(A_1) - \omega(E_1)$ (c) for both PMN and PMT. The dashed lines are guides for the eyes.

constitutes a measurement of the E_1 component. Indeed, the frequency compares very well to that extracted from IR [45], at least in PMN.

Owing to the preceding, we used a Breit-Wigner-Fano (BWF) formula [62,63] and a sloping background to fit the data in PMN. To avoid dispersion in the fitting parameters, the asymmetry factor α was kept constant for all temperatures. This asymmetric function reproduces well the data over the whole investigated temperature range, and the resulting frequencies at the maximum of the band (full symbols) are plotted in Fig. 6. A weak anomaly is seen near the freezing temperature T_f , that is, the temperature at which a ferroelectric phase transition is observed under an applied electric field [25]. In our experiments, no external field was applied, but the strong light source incoming onto the sample could eventually induce displacements and thus acts as an applied external electric field. However, our HRS spectra are so similar to those extracted from IR at zero field [45] that this effect, if it exists, can be neglected. To confirm this observation, another high-resolution set of data was performed on the same PMN sample in the temperature interval between 185 and 230 K with a 5 K step. The same fitting model was used to

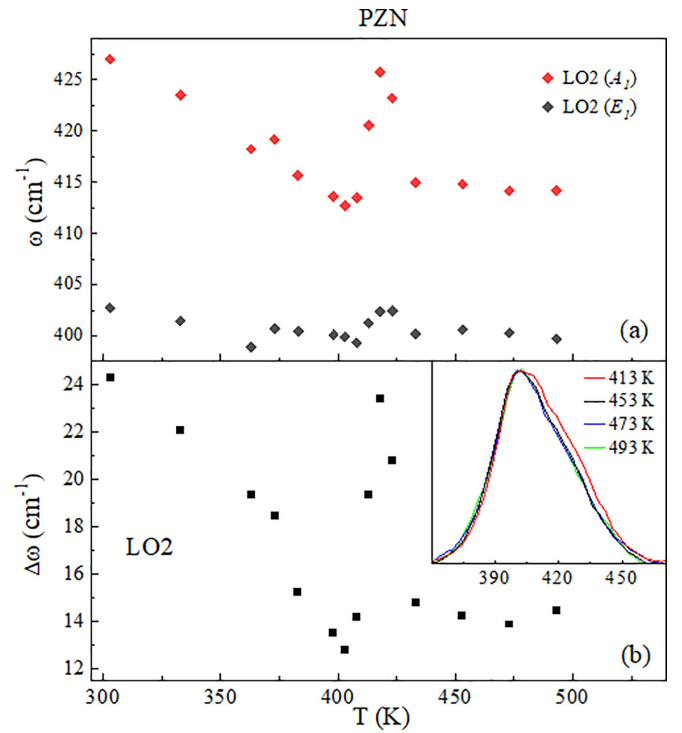


FIG. 5. Temperature dependence of the E_1 and A_1 (a) and $\Delta\omega = \omega(A_1) - \omega(E_1)$ (b) for PZN. The inset shows the evolution of the A_1 component near T_m .

extract the peak maximum, and the results are shown by the open symbols in Fig. 6. The two sets of data overlap at identical temperatures ensuring that these results are reproducible. The frequency of the E_1 component of LO1 exhibits a sharp transition-like feature near $T_f \approx 220$ K. This effect can be directly seen from the raw data presented in the inset of Fig. 6.

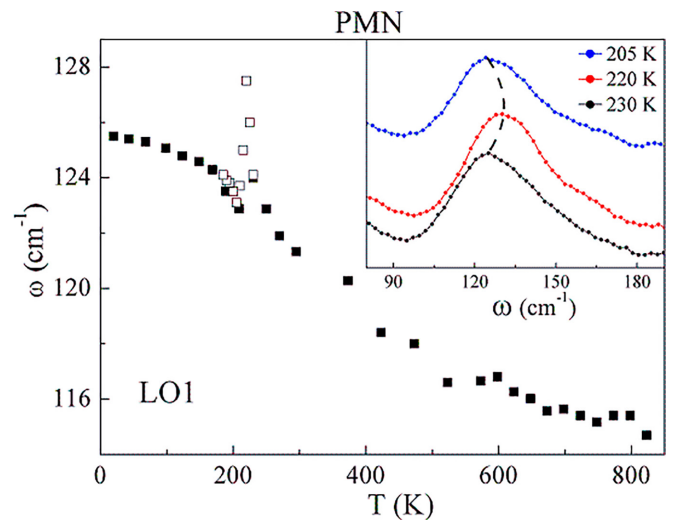


FIG. 6. Temperature dependence of the frequency of the E_1 component of LO1 in PMN. The empty symbols represent the frequencies obtained from another high-resolution experiment performed on the same PMN sample in the temperature interval between 185 and 230 K. The inset shows the HRS spectra at three different temperatures surrounding $T_f \approx 220$ K.

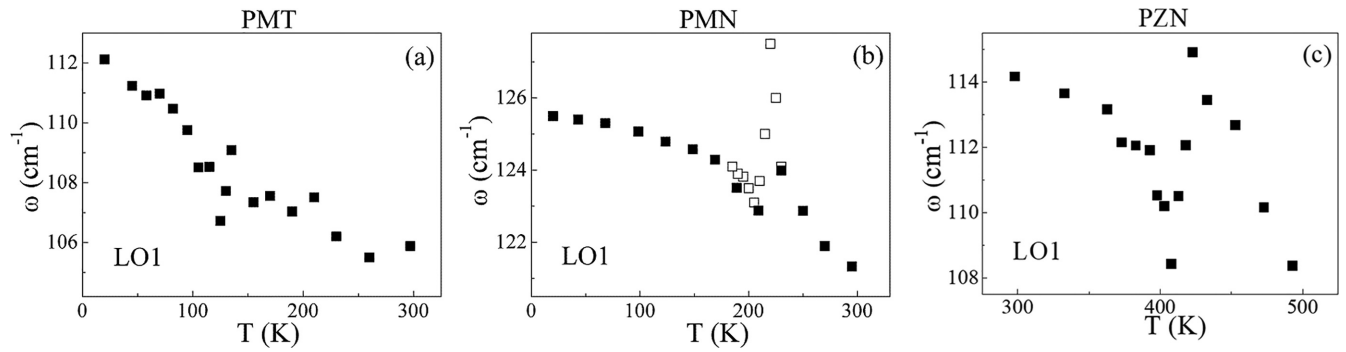


FIG. 7. Temperature dependence of the frequency of the E_1 component of the LO1 mode of PMT (a), PMN (b), and PZN (c). The empty symbols in (b) represent the frequencies obtained from another high-resolution experiment performed on the same PMN sample in the temperature interval between 185 and 230 K.

To fit the LO1 mode in PMT and PZN, it is preferable to use a Gaussian-asymmetric function

$$I(\omega) = I_0 \exp\left[-\frac{1}{2}\left(\frac{\omega-\omega_0}{\sigma+\alpha\sqrt{\omega-\omega_0}}\right)^2\right] \times [n(\omega) + 1],$$

where ω_0 is the peak frequency, σ is the Gaussian width, I_0 is the peak intensity, and α is a coefficient relating to the degree of asymmetry of the line. This function provides better fits than the BWF function used previously in PMN. Similar results (although more dispersed) can be obtained by a simple fit of the points around the maximum with a polynomial function. The results for the three samples are summarized in Fig. 7. A transition-like feature on LO1(E_1) is observed in PMN and PZN, but not in PMT. In PZN, the anomaly is similar to that observed on LO2 and most likely associates with the long-range paraelectric-ferroelectric phase transition. Finally in PMT, no field-induced ferroelectric phase transition has been reported near the temperature corresponding to the maximum of ϵ (≈ 170 K) [28], and our results on LO1 do not show any anomaly in that temperature range [Fig. 7(a)].

D. Discussion

Within the framework of the simple eigenvector model described in the work of Hlinka *et al.* [47], the eigenvectors for the three F_{1u} modes apply for the three TOs, but it is not clear whether this picture is true for the LOs. However, it is tempting to relate the sharp anomaly on LO1(E_1) in PMN at $T_f \approx 220$ K to the hardening of the soft TO1 mode observed in RS below T_f [64]. In addition, we have shown in a previous work that the nonpolar F_{2u} vibration has a normal temperature behavior [60]. This probably means that the oxygen atoms play a minor role in the structural modifications of cubic relaxors. As LO3 exhibits the weakest anomalies with temperature, its eigenvectors likely involve preferentially the oxygen atoms. This corresponds to the Axe mode [47] which associates to the hardest F_{1u} -symmetry vibration (TO3). These general considerations suggest that TO $_i$ associates with LO $_i$ ($i = 1,2,3$) in cubic lead-based relaxors. Contrary to PZN, there is no long-range order transition at T_f in PMN. This is probably the reason the sharp anomaly observed at T_f in the latter is not reproduced by any other LO mode (nor F_{2u}). From the simple eigenvectors description [47], the lead atoms have the major weight in the low-frequency F_{1u} vibration (Last

mode [47]). It is thus likely that this transition-like anomaly relates to a local peculiar behavior (in the PNRs ?) at the A site keeping the average structure unchanged. Indeed, the long-range ordering in PZN translates into a sharp maximum of the SHG signal around $T_f \approx 385$ K [Fig. 8(b)]. On the contrary, the continuous increase of the SHG in PMN [Fig. 8(a)] rather

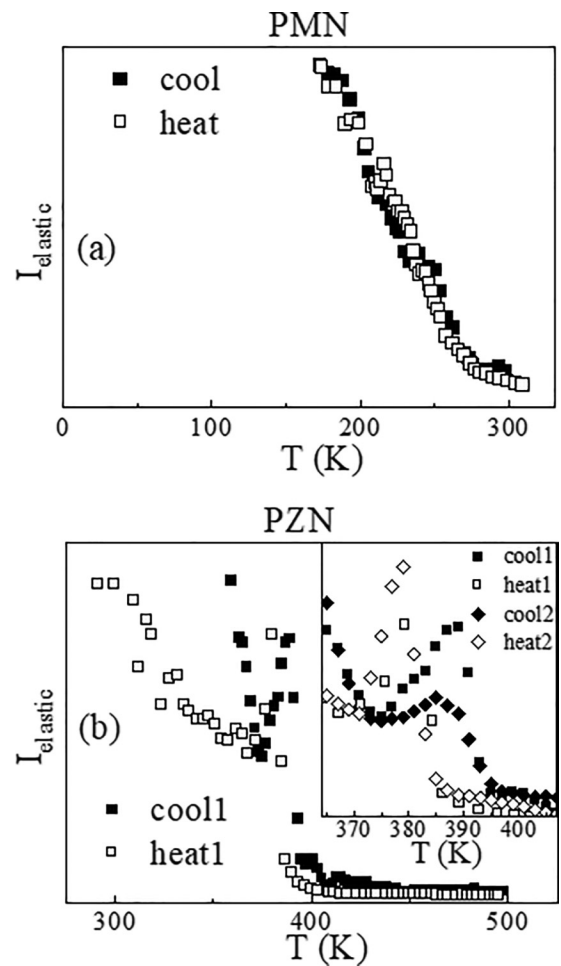


FIG. 8. The SHG (elastic contribution in HRS) as a function of temperature in PMN (a) and PZN (b) emphasizing a sharp maximum at $T_f \approx 385$ K in the latter. The inset shows the hysteresis behavior of the SHG signal in PZN.

supports the idea of local distortions in the disordered PNRs. Still, within our simple eigenvector description, LO2 should associate to the Slater mode [47].

Assuming that oxygens are weakly involved in the structural process, the hardening and the strong intensity increase of the LO2(A_1) component in PMN and PMT (Figs. 3 and 4) could thus be related to either a growth of a polarization component on the B site between T_d and T_m or to an increase of the polar ordering of the B atoms within the PNRs, or both. In PMN and PMT, the splitting remains well above T_d , showing that the structural disorder persists up to the highest temperature measured (~ 750 K). It is more pronounced in PMT than in PMN, and very weak in PZN. We conclude that the shape of the LO2 doublet could provide an indirect way to get information on the local structural disorder (most likely at the B site). It seems from these results that the bigger the splitting, the higher the structural distortions and frustration, and the lower the value of the dielectric constant at T_m (at 100 kHz, $\epsilon_{PMT} \approx 5000$ [29], $\epsilon_{PMN} \approx 12,000$ [24], and $\epsilon_{PZN} \approx 45,000$ [34]).

IV. CONCLUSIONS

LO modes of three lead-based ferroelectric relaxors PMN, PMT, and PZN are obtained using HRS spectroscopy. Three

asymmetric and broad LO peaks are seen in the three materials corresponding to LO1 near 110 cm^{-1} , LO2 around 400 cm^{-1} , and LO3 centered around 700 cm^{-1} . In PZN, the long-range order paraelectric-ferroelectric transition is seen by sharp anomalies near T_m in the temperature dependence of LO1 and LO2. In PMN, this transition-like anomaly is only observed for LO1 at T_f . A possible explanation could be that local distortions involving (mainly) the lead atoms develop in the PNRs below T_f . The other modes are not (or at least much less) affected because this effect does not translate into a long-range order state and the PNRs remain randomly oriented. This observation, together with that of a ferroelectric transition under an electric field at T_f , suggests that at a zero field, PMN is very close to instability. In PMT where the local distortions are larger, there is no T_f (no evidence for a field-induced ferroelectric phase transition) and no transition-like anomaly on the LO modes was evidenced. Our HRS spectroscopy shows that the structural disorder increases from PZN to PMN to PMT, and that this disorder prevents long-range ordering at low temperature.

ACKNOWLEDGMENT

The authors would like to thank Dr. J. Hlinka for providing the samples and for fruitful discussions.

-
- [1] C. Qi, Y. Jiang, X. Wang, and C. S. Lynch, Phase transition by nanoindentation in a relaxor ferroelectric single crystal PMN-0.3PT: A phase-field investigation, *J. Appl. Phys.* **131**, 244101 (2022).
- [2] N. Kumar, X. Shi, and M. Hoffman, Spontaneous relaxor to ferroelectric transition in lead-free relaxor piezoceramics and the role of point defects, *J. Eur. Ceram. Soc.* **40**, 2323 (2020).
- [3] R. A. Cowley, S. N. Gvasaliya, S. G. Lushnikov, B. Roessli, and G. M. Rotarum, Relaxing with relaxors: A review of relaxor ferroelectrics, *Adv. Phys.* **60**, 229 (2011).
- [4] L. L. Zhang and Y. N. Huang, Theory of relaxor-ferroelectricity, *Sci. Rep.* **10**, 5060 (2020).
- [5] T. Rojac, Piezoelectric response of disordered lead-based relaxor ferroelectrics, *Commun. Mater.* **4**, 12 (2023).
- [6] A. D. Ushakov, Q. Hu, X. Liu, Z. Xu, X. Wei, and V. Y. Shur, Triple and double hysteresis loops in relaxor ferroelectric PMN-0.28PT crystals, *Ferroelectrics* **604**, 91 (2023).
- [7] P. Vijayakumar, C. Manikandan, R. M. Sarguna, E. P. Amaladass, K. Ganesan, V. Roy, E. Varadarajan, and S. Ganesamoorthy, Growth of large-sized relaxor ferroelectric PZN-PT single crystals by modified flux growth method, *J. Cryst. Growth* **626**, 127462 (2024).
- [8] M. Kopecky, J. Kub, J. Fabry, and J. Hlinka, Nanometer-range atomic order directly recovered from resonant diffuse scattering, *Phys. Rev. B* **93**, 054202 (2016).
- [9] A. Al-Barakaty, S. Prosandeev, D. Wang, B. Dkhil, and L. Bellaiche, Finite-temperature properties of the relaxor $\text{PbMg}_{1/3}\text{Nb}_{2/3}\text{O}_3$ from atomistic simulations, *Phys. Rev. B* **91**, 214117 (2015).
- [10] G. Burns and B. A. Scott, Index of refraction in ‘dirty’ displacive ferroelectrics, *Solid State Commun.* **13**, 423 (1973).
- [11] O. Aktas, M. Kangama, G. Linyu, X. Ding, M. A. Carpenter, and E. K. H. Salje, Probing the dynamic response of ferroelectric and ferroelastic materials by simultaneous detection of elastic and piezoelectric properties, *J. Alloys Compd.* **903**, 163857 (2022).
- [12] A. A. Bokov and Z.-G. Ye, Recent progress in relaxor ferroelectrics with perovskite structure, *J. Mater. Sci.* **41**, 31 (2006).
- [13] L. M. Riemer, K. Chu, Y. Li, H. Ursic, A. J. Bell, B. Dkhil, and D. Damjanovic, Macroscopic polarization in the nominally ergodic relaxor state of lead magnesium niobate, *Appl. Phys. Lett.* **117**, 102901 (2020).
- [14] G. A. Samara, Ferroelectricity revisited—Advances in materials and physics, *Solid State Physics* (Academic, New York, 2001), Vol. 56, p. 240.
- [15] P. Ondrejko, M. Kempa, J. Kulda, B. Frick, M. Appel, J. Combet, J. Dec, T. Lukasiewicz, and J. Hlinka, Dynamics of nanoscale polarization fluctuations in a uniaxial relaxor, *Phys. Rev. Lett.* **113**, 167601 (2014).
- [16] D. Viehland, S. J. Jang, L. E. Cross, and M. Wuttig, Deviation from Curie-Weiss behavior in relaxor ferroelectrics, *Phys. Rev. B* **46**, 8003 (1992).
- [17] M. V. Takarkhede and S. A. Band, Large dielectric response of 0.6PMN-0.4PZN relaxor ferroelectric ceramic for multilayer capacitors, *Ferroelectrics Lett.* **46**, 111 (2019).
- [18] J. Macutkevicius, S. Kamba, K. Glemza, J. Banys, K. Bormanis, and A. Sternberg, High temperature dielectric properties of PMN-PSN-PZN relaxors, *Phys. Status Solidi B* **256**, 1900050 (2019).
- [19] D. Nuzhnyy, J. Petzelt, V. Bovtun, S. Kamba, and J. Hlinka, Soft mode driven local ferroelectric transition in lead-based relaxors, *Appl. Phys. Lett.* **114**, 182901 (2019).

- [20] O. Aktas and E. K. H. Salje, Macroscopic symmetry breaking and piezoelectricity in relaxor ferroelectric lead magnesium niobate, *Appl. Phys. Lett.* **113**, 202901 (2018).
- [21] G. Burns and F. H. Dacol, Glassy polarization behavior in ferroelectric compounds $\text{Pb}(\text{Mg}_{1/3}\text{Nb}_{2/3})\text{O}_3$ and $\text{Pb}(\text{Zn}_{1/3}\text{Nb}_{2/3})\text{O}_3$, *Solid State Commun.* **48**, 853 (1983).
- [22] L. E. Cross, Relaxor ferroelectrics, *Ferroelectrics* **76**, 241 (1987).
- [23] B. Dkhil, P. Gemeiner, A. Al-Barakaty, L. Bellaiche, E. Dul'kin, E. Mojaev, and M. Roth, Intermediate temperature scale T^* in lead-based relaxor systems, *Phys. Rev. B* **80**, 064103 (2009).
- [24] V. Bovtun, S. Veljko, S. Kamba, J. Petzelt, S. Vakhrushev, Y. Yakymenko, K. Brinkman, and N. Setter, Broad-band dielectric response of $\text{PbMg}_{1/3}\text{Nb}_{2/3}\text{O}_3$ relaxor ferroelectrics: Single crystals, ceramics and thin films, *J. Eur. Ceram. Soc.* **26**, 2867 (2006).
- [25] G. Schmidt, H. Arndt, J. Voncieminski, T. Petzsche, H. Voigt, and N. N. Krainik, Field-induced phase transition in lead magnesium niobate, *Krist. Tech.* **15**, 1415 (1980).
- [26] V. Sivasubramanian and S. Ganesamoorthy, Elastic behavior and dynamical aspects of polarization in $\text{Pb}(\text{Mg}_{1/3}\text{Nb}_{2/3})\text{O}_3$ and $\text{Pb}(\text{Mg}_{1/3}\text{Ta}_{2/3})\text{O}_3$ studied by Brillouin spectroscopy, *Eur. Phys. J. Appl. Phys.* **69**, 10701 (2015).
- [27] S. N. Gvasaliya, V. Pomjakushin, B. Roessli, T. Strässle, S. Klotz, and G. S. Lushnikov, Anomalous pressure dependence of the atomic displacements in the relaxor ferroelectric $\text{PbMg}_{1/3}\text{Ta}_{2/3}\text{O}_3$, *Phys. Rev. B* **73**, 212102 (2006).
- [28] S. N. Gvasaliya, B. Roessli, D. Sheptyakov, S. G. Lushnikov, and T. A. Shaplygina, Neutron scattering study of $\text{PbMg}_{1/3}\text{Ta}_{2/3}\text{O}_3$ and $\text{BaMg}_{1/3}\text{Ta}_{2/3}\text{O}_3$ complex perovskites, *Eur. Phys. J. B* **40**, 235 (2004).
- [29] J.-H. Ko, S. Kojima, and S. G. Lushnikov, Different dynamic behaviors of $\text{Pb}(\text{Mg}_{1/3}\text{Ta}_{2/3})\text{O}_3$ and $\text{Ba}(\text{Mg}_{1/3}\text{Ta}_{2/3})\text{O}_3$ single crystals studied by micro-Brillouin scattering and dielectric spectroscopy, *Appl. Phys. Lett.* **82**, 4128 (2003).
- [30] S. G. Lushnikov, J.-H. Ko, and S. Kojima, Anomalous field-induced effects in the sound velocity in lead magnesium niobate probed by micro-Brillouin scattering, *Appl. Phys. Lett.* **84**, 4798 (2004).
- [31] S. G. Lushnikov, A. I. Fedoseev, S. N. Gvasaliya, and S. Kojima, Anomalous dispersion of the elastic constants at the phase transformation of the $\text{PbMg}_{1/3}\text{Nb}_{2/3}\text{O}_3$ relaxor ferroelectric, *Phys. Rev. B* **77**, 104122 (2008).
- [32] Y. L. Wang, S. S. N. Bharadwaja, A. K. Tagantsev, and N. Setter, Dielectric properties of 1:1 ordered $\text{Pb}(\text{Mg}_{1/3}\text{Ta}_{2/3})\text{O}_3$ ceramics, *J. Eur. Ceram. Soc.* **25**, 2521 (2005).
- [33] T. R. Welberry, Lead perovskite relaxors, PZN and PMN, in *Diffuse X-ray Scattering and Models of Disorder*, 2nd ed. (Oxford University Press, Oxford, 2022), Chap. 23, pp. 330–365.
- [34] A. Lebon, H. Dammak, and G. Calvarin, Tetragonal and rhombohedral induced polar order from the relaxor state of $\text{PbZn}_{1/3}\text{Nb}_{2/3}\text{O}_3$, *J. Phys.: Condens. Matter* **15**, 3069 (2003).
- [35] Y. Yokomizo, T. Takahashi, and S. Nomura, Ferroelectric properties of $\text{Pb}(\text{Zn}_{1/3}\text{Nb}_{2/3})\text{O}_3$, *J. Phys. Soc. Jpn.* **28**, 1278 (1970).
- [36] S. Nomura, M. Endo, and F. Kojima, Ferroelectric domains and polarization reversal in $\text{Pb}(\text{Zn}_{1/3}\text{Nb}_{2/3})\text{O}_3$ crystal, *Jpn. J. Appl. Phys.* **13**, 2004 (1974).
- [37] A. Lebon, H. Dammak, G. Calvarin, and I. O. Ahmedou, The cubic-to-rhombohedral phase transition of $\text{Pb}(\text{Zn}_{1/3}\text{Nb}_{2/3})\text{O}_3$: A high-resolution x-ray diffraction study on single crystals, *J. Phys.: Condens. Matter* **14**, 7035 (2002).
- [38] G. Xu, Z. Zhong, Y. Bing, Z.-G. Ye, C. Stock, and G. Shirane, Ground state of the relaxor ferroelectric $\text{Pb}(\text{Zn}_{1/3}\text{Nb}_{2/3})\text{O}_3$, *Phys. Rev. B* **67**, 104102 (2003).
- [39] G. Xu, Z. Zhong, Y. Bing, Z.-G. Ye, C. Stock, and G. Shirane, Anomalous phase in the relaxor ferroelectric $\text{Pb}(\text{Zn}_{1/3}\text{Nb}_{2/3})\text{O}_3$, *Phys. Rev. B* **70**, 064107 (2004).
- [40] P. M. Gehring, S. Wakimoto, Z.-G. Ye, and G. Shirane, Soft mode dynamics above and below the Burns temperature in the relaxor $\text{Pb}(\text{Mg}_{1/3}\text{Nb}_{2/3})\text{O}_3$, *Phys. Rev. Lett.* **87**, 277601 (2001).
- [41] S. N. Gvasaliya, B. Roessli, R. A. Cowley, P. Huber, and S. G. Lushnikov, Quasi-elastic scattering, random fields and phonon-coupling effects in $\text{PbMg}_{1/3}\text{Nb}_{2/3}\text{O}_3$, *J. Phys.: Condens. Matter* **17**, 4343 (2005).
- [42] O. Svitelskiy, J. Toulouse, G. Yong, and Z.-G. Ye, Polarized Raman study of the phonon dynamics in $\text{Pb}(\text{Mg}_{1/3}\text{Nb}_{2/3})\text{O}_3$ crystal, *Phys. Rev. B* **68**, 104107 (2003).
- [43] J.-H. Ko, D. H. Kim, and S. Kojima, Central peaks, acoustic modes, and the dynamics of polar nanoregions in $\text{Pb}[(\text{Zn}_{1/3}\text{Nb}_{2/3})_x\text{Ti}_{1-x}]\text{O}_3$ single crystals studied by Brillouin spectroscopy, *Phys. Rev. B* **77**, 104110 (2008).
- [44] J. Toulouse, F. Jiang, O. Svitelskiy, W. Chen, and Z.-G. Ye, Temperature evolution of the relaxor dynamics in $\text{Pb}(\text{Zn}_{1/3}\text{Nb}_{2/3})\text{O}_3$: A critical Raman analysis, *Phys. Rev. B* **72**, 184106 (2005).
- [45] J. Hlinka, T. Ostapchuk, D. Noujni, S. Kamba, and J. Petzelt, Anisotropic dielectric function in polar nanoregions of relaxor ferroelectrics, *Phys. Rev. Lett.* **96**, 027601 (2006).
- [46] S. Kamba, D. Nuzhnyy, S. Veljko, V. Bovtun, J. Petzelt, Y. L. Wang, N. Setter, J. Levoska, M. Tyunina, J. Macutkevicius, and J. Banys, Dielectric relaxation and polar phonon softening in relaxor ferroelectric $\text{PbMg}_{1/3}\text{Ta}_{2/3}\text{O}_3$, *J. Appl. Phys.* **102**, 074106 (2007).
- [47] J. Hlinka, J. Petzelt, S. Kamba, D. Noujni, and T. Ostapchuk, Infrared dielectric response of relaxor ferroelectrics, *Phase Transit.* **79**, 41 (2006).
- [48] A. Al-Zein, J. Hlinka, J. Rouquette, and B. Hehlen, Soft mode doublet in $\text{PbMg}_{1/3}\text{Nb}_{2/3}\text{O}_3$ relaxor investigated with hyper-Raman scattering, *Phys. Rev. Lett.* **105**, 017601 (2010).
- [49] A. Al-Zein, J. Hlinka, J. Rouquette, A. Kania, and B. Hehlen, Hyper-Raman scattering: New prospects for the description of the local structure of complex perovskites, *J. Appl. Phys.* **109**, 124114 (2011).
- [50] H. Vogt and G. Rossbroich, Accurate determination of the far-infrared dispersion in SrTiO_3 by hyper-Raman spectroscopy, *Phys. Rev. B* **24**, 3086 (1981).
- [51] B. Hehlen, M. Al-Sabbagh, A. Al-Zein, and J. Hlinka, Relaxor ferroelectrics: Back to the single-soft-mode picture, *Phys. Rev. Lett.* **117**, 155501 (2016).
- [52] J. Hlinka, B. Hehlen, A. Kania, and I. Gregora, Soft mode in cubic PbTiO_3 by hyper-Raman scattering, *Phys. Rev. B* **87**, 064101 (2013).
- [53] N. Dhifallah, B. Hehlen, and H. Khemakhem, Hyper-Raman scattering study of the soft mode in relaxor ferroelectric $(\text{Ba}_{0.8}\text{Sr}_{0.2})_{0.925}\text{Bi}_{0.05}\text{Ti}_{0.95}(\text{Zn}_{1/3}\text{Nb}_{2/3})_{0.05}\text{O}_3$, *J. Raman Spectrosc.* **53**, 1148 (2022).

- [54] V. N. Denisov, B. N. Marvin, and V. B. Podobedov, Hyper-Raman scattering by vibrational excitations in crystals, glasses and liquids, *Phys. Rep.* **151**, 1 (1987).
- [55] S. J. Cyvin, J. E. Rauch, and J. C. Decius, Theory of hyper-Raman effects (nonlinear inelastic light scattering): Selection rules and depolarization ratios for the second-order polarizability, *J. Chem. Phys.* **43**, 4083 (1965).
- [56] G. Simon, B. Hehlen, R. Vacher, and E. Courtens, Nature of the hyper-Raman active vibrations of lithium borate glasses, *J. Phys.: Condens. Matter* **20**, 155103 (2008).
- [57] B. Hehlen, A. Al-Zein, C. Bogicevic, P. Gemeiner, and J.-M. Kiat, Soft-mode dynamics in micrograin and nanograin ceramics of strontium titanate observed by hyper-Raman scattering, *Phys. Rev. B* **87**, 014303 (2013).
- [58] B. Hehlen, A. Amouri, A. Al-Zein, and H. Khemakhem, Hyper-Raman and Raman scattering from the polar modes of $\text{PbMg}_{1/3}\text{Nb}_{2/3}\text{O}_3$, *J. Phys.: Condens. Matter* **26**, 015401 (2014).
- [59] H. Hellwig, A. Sehirlioglu, D. A. Payne, and P. Han, Hyper-Raman-active soft mode in $\text{Pb}(\text{Mg}_{1/3}\text{Nb}_{2/3})_{0.73}\text{Ti}_{0.27}\text{O}_3$, *Phys. Rev. B* **73**, 094126 (2006).
- [60] A. Al-Zein, B. Hehlen, J. Rouquette, and J. Hlinka, Polarized hyper-Raman scattering study of the silent F_{2u} mode in $\text{PbMg}_{1/3}\text{Nb}_{2/3}\text{O}_3$, *Phys. Rev. B* **78**, 134113 (2008).
- [61] B. Hehlen, G. Simon, and J. Hlinka, Polar modes in relaxor $\text{PbMg}_{1/3}\text{Nb}_{2/3}\text{O}_3$ by hyper-Raman scattering, *Phys. Rev. B* **75**, 052104 (2007).
- [62] J. F. Scott, Soft-mode spectroscopy: Experimental studies of structural phase transitions, *Rev. Mod. Phys.* **46**, 83 (1974).
- [63] M. R. Dresselhaus and G. Dresselhaus, Intercalation compounds of graphite, *Adv. Phys.* **30**, 139 (1981).
- [64] D. Fu, H. Taniguchi, M. Itoh, S.-Y. Koshihara, N. Yamamoto, and S. Mori, Relaxor $\text{Pb}(\text{Mg}_{1/3}\text{Nb}_{2/3})\text{O}_3$: A ferroelectric with multiple inhomogeneities, *Phys. Rev. Lett.* **103**, 207601 (2009).